Carbohydrate Polymers 99 (2014) 710–719

Contents lists available at ScienceDirect

Carbohydrate Polymers

journal homepage: www.elsevier.com/locate/carbpol

Amphiphilic polyesters bearing pendant sugar moieties: Synthesis, characterization, and cellular uptake

Kang-Yu Peng[a], Mu-Yi Hua[b], Ren-Shen Lee[a,*]

[a] Division of Nature Science, Center of General Education, Chang Gung University, 259 Wen-Hwa 1st Road, Kwei-Shan, Tao-Yuan 333, Taiwan, ROC
[b] Department of Chemical and Materials Engineering, Chang Gung University, Tao-Yuan, Taiwan

ARTICLE INFO

Article history:
Received 20 June 2013
Received in revised form 20 August 2013
Accepted 25 August 2013
Available online 8 September 2013

Keywords:
Glycopolymer
Block-graft polymer
Cellular uptake
Drug delivery

ABSTRACT

Ring-opening polymerization (ROP) and "click" reactions were used to prepare a series of amphiphilic block-graft (PαN$_3$CL-g-Sugar)-*b*-PCL polymers. The glycosylated RO-(PαN$_3$CL-g-Sugar)-*b*-PCL polymers formed micelles with critical micelle concentrations (CMCs) in the range of 4.9–23.2 mg L^{-1} in the aqueous phase. The mean diameters of the micelles were between 21 nm and 125 nm, considerably lower than the 200 nm diameter at which the uptake of micelles by the reticuloendothelial cells becomes compromised. Selective lectin-binding experiments confirmed that glycosylated RO-(PαN$_3$CL-g-Sugar)-*b*-PCL can be used in biorecognition applications, and in vitro cell-viability assay showed that RO-(PαN$_3$CL-g-Sugar)-*b*-PCL has low cytotoxicity. Micelles loaded with doxorubicin (DOX) facilitated an improved uptake of DOX by HeLa cells that was completed within 1 h, and the endocytosed-DOX successfully reached intracellular compartments and entered nuclei.

1. Introduction

The self-association of amphiphilic block copolymers into supramolecular assemblies, which is well documented (Moughton, Hillmyer, & Lodge, 2011; Tunca, 2013), is attracting growing interest because of the application of the self-association property in functional nanofabricated materials (Jutz & Böker, 2011; Torchilin, 2007). In selected solvents, amphiphilic block copolymers form polymeric micelles and aggregates that consist of a core made of the insoluble parts of the macromolecules surrounded by a shell of solvated "block". Polymeric micelles and aggregates can potentially deliver hydrophobic drugs and bioactive molecules into cells (Mikhail & Allen, 2009; Tyrrell, Shen, & Radosz, 2010), but one major challenge is the method of development that enable the micelles to recognize and bind specific cellular targets (Rajendran, Knölker, & Simons, 2010; Sunasee & Narain, 2013).

Synthetic polymers bearing carbohydrate groups in the side chains or at the ends of macromolecular chains, called glycopolymers, have been widely studied for potential applications in the fields of biomedicine and biomaterials (Cerrada et al., 2013; Kim et al., 2013). Of particular interest are biocompatible polyesters containing cyclic saccharides that potentiate multivalent protein–carbohydrate interactions in living organisms, which facilitate biomolecular recognition events that differ dramatically from the recognition elicited by monovalent interactions (Bertozzi & Kiessling, 2001; Bordege, Munoz-Bonilla, Cuervo-Rodriguez, Sanchez-Chaves, & Fernandez-Garcia, 2011). Therefore, considerable research on glycopolymers has focused on developing lectin targets (Ting, Chen, & Stenzei, 2010) and drug-delivery systems (Polikarpov, Kaufmann, Kluge, Appelhans, & Voit, 2010; Top & Kiick, 2010).

Glycopolymers can be synthesized by polymerizing carbohydrate-linked monomers or by glycosylating polymers (Menon & Das, 2012; Krannig & Schlaad, 2012; Jubeli, Moine, & Barratt, 2010; Xiao et al., 2010); in both cases, the chain-length of the polymers and the carbohydrate density of the back-bone can be tightly controlled using atom transfer radical polymerization. Synthetic glycopolymers with biocompatible and biodegradable properties are increasingly being used in tissue engineering and controlled drug-delivery applications (Huang, Habraken, Audouin, & Heise, 2010; Lee & Peng, 2012; Lu et al., 2007). In this study, we synthesized an amphiphilic biodegradable or bioresorbable sugar-linked poly(ε-caprolactone) (PCL) copolymer as a novel precursor for colloidal drug-delivery systems. The copolymer consists of a bio-recognizable PαN$_3$CL-g-Sugar that bears pendant sugars as the hydrophilic segment, and the biocompatible PCL as the hydrophobic segment. We investigated the amphiphilicity and self-assembly of the copolymer and the recognition of the copolymer by a glucose-specific lectin.

* Corresponding author. Tel.: +886 3 211 8800 5054.
E-mail address: shen21@mail.cgu.edu.tw (R.-S. Lee).

0144-8617/$ – see front matter © 2013 Elsevier Ltd. All rights reserved.
http://dx.doi.org/10.1016/j.carbpol.2013.08.098

2. Experimental methods

2.1. Synthesis of RO-(PαN$_3$CL-g-Sugar)-b-PCL grafted polymers

All glass containers used were oven-dried and handled under a dry N_2 stream. The copolymer RO-(PαN$_3$CL-g-Sugar)-*b*-PCL was synthesized as follows. The initiator 1-pyrenemethanol (or benzyl alcohol) (0.765 mmol), and αClCL (7.65 mmol) were mixed in a flask, heated under a dry N_2 stream, and dissolved in 50 mL of toluene, following which 25 mg of $SnOct_2$ (1.5 wt% based on the weight of the initiator and αClCL) was added. The flask was purged with N_2 and refluxed for 24 h, and the resulting product, RO-PαClCL, was dissolved in $CHCl_3$, and precipitated into excess *n*-hexane/diethyl ether (v/v 5:1) with stirring. The purified polymer was dried under vacuum at 50 °C for 24 h and then analyzed. ^{1}H NMR ($CDCl_3$): δ 8.35–8.0 (m, $C_{16}H_9$—), 5.22 (s, $C_{16}H_9CH_2$—), 4.29 (m, $C_\alpha ClH$—), 4.20 (m, $C_\varepsilon H_2O$—), 2.02 (m, $C_\beta H_2$—), 1.73 (m, $C_\delta H_2$—), 1.57 (m, $C_\gamma H_2$—).

The macroinitiator PMO-PαClCL$_{16}$, was used to trigger the polymerization of ε-CL. PMO-PαClCL$_{16}$ (M_n = 2610 mg mol^{-1}, 0.17 mmol) and ε-CL (5.1 mmol) were mixed in a flask under a dry N_2 stream, after which 22 mg of $SnOct_2$ (1.5 wt% based on the weight of PMO-PαClCL$_{16}$ and ε-CL) and toluene (30 mL) were added. The flask was purged with N_2 and the reaction solution was refluxed for 24 h and then-concentrated under vacuum in a rotary evaporator. The product was dissolved in $CHCl_3$ and precipitated into excess *n*-hexane/diethyl ether (v/v 5:1) with stirring. The purified polymer was dried under vacuum at 50 °C for 24 h and then analyzed. ^{1}H NMR ($CDCl_3$): δ 8.35–8.0 (m, $C_{16}H_9$—), 5.22 (s, $C_{16}H_9CH_2$—), 4.26 (m, $C_\alpha ClH$— of PαClCL), 4.18 (m, $C_\varepsilon H_2O$— of PαClCL), 4.08 (m, $C_\varepsilon H_2O$— of PCL), 2.33 (t, J = 7.2 Hz, $C_\alpha H_2$— of PCL), 2.13 (m, $C_\beta H_2$— of PαClCL), 1.64 (m, $C_\delta H_2$— of PαClCL, and $C_\beta H_2$— and $C_\delta H_2$— of PCL), 1.37 (m, $C_\gamma H_2$— of PαClCL and PCL).

PMO-PαClCL$_{16}$-*b*-PCL$_{34}$ (0.22 mmol, 16 equiv. of αClCL) was dissolved in 10 mL of *N,N*-dimethylformamide (DMF) in a glass reactor, NaN_3 (3.87 mmol) was added, and the mixture was stirred overnight at room temperature. After filtering out the insoluble salt and eliminating DMF under vacuum, the product was dissolved in $CHCl_3$ and precipitated into excess *n*-hexane/diethyl ether (v/v 4:1) with stirring. The purified polymer was dried under vacuum at 50 °C for 24 h and then analyzed. Fig. 1A shows a representative ^{1}H NMR spectrum of PMO-PαN$_3$CL$_{16}$-*b*-PCL$_{34}$, and Fig. S1B (in supporting information) shows a representative FT-IR spectrum of PMO-PαN$_3$CL$_{16}$-*b*-PCL$_{34}$.

In the final step of the copolymer synthesis, PMO-PαN$_3$CL$_{16}$-*b*-PCL$_{34}$ (27.9 mmol, 0.45 mol equiv. of azide) was transferred into a glass reactor containing THF and then 1-(4-pentynyl)-glucose (0.45 mol), CuI (2.8 mmol), and triethyl amine (2.8 mmol) were added. The solution was stirred at 60 °C for 48 h and the reaction product was cooled and precipitated in diethyl ether. The purified polymer was dried under vacuum at 50 °C for 24 h and then analyzed. Fig. 1B shows a representative ^{1}H NMR spectrum of PMO-(PαN$_3$CL$_{16}$-*g*-Gluco$_{13}$)-*b*-PCL$_{34}$, and Fig. S1C (in supporting information) shows a representative FT-IR spectrum of PMO-(PαN$_3$CL$_{16}$-*g*-Gluco$_{13}$)-*b*-PCL$_{34}$.

2.2. In vitro drug-release studies

Various micelles loaded with indomethacin (IMC) were weighted out (exactly 110.2 mg) and suspended in 10 mL of phosphate buffer solution (PBS) (0.1 M, pH 7.4). The micellar solution was transferred to a dialysis membrane bag (MWCO = 3500), which was placed in 50 mL of PBS (release medium) and gently stirred (30 rpm) at 37 °C. At predetermined time intervals, 3 mL aliquots of the release medium were withdrawn, and replaced with an equal volume of fresh PBS. The concentration of IMC released into PBS was measured using a UV-Vis spectrophotometer at 320 nm to generate a calibration curve, and the controlled drug-release rate was calculated using the total released weight of IMC in relation to the calibration curve.

2.3. Carbohydrate-lectin binding assay

The lectin-binding activity of the PMO-(PαN$_3$CL-*g*-Gluco)-*b*-PCL solution was analyzed by the change in turbidity at 450 nm at room temperature. A 2 mg mL^{-1} sample of the lectin Concanavalin- A (Con A) was prepared in 0.01 M PBS, pH 7.4, and 600 μL of the Con A solution was transferred into a cuvette to measure the absorbance baseline. Next, 60 μL of RO-(PαN$_3$CL-*g*-Gluco)-*b*-PCL, either 0.1 or 0.2 mg mL^{-1} in PBS, was added to the Con A in the cuvette and the solution was mixed gently by a pipetting; immediately thereafter, the absorbance of the solution at 450 nm was recorded every 200 s. As a control, PBS without RO-(PαN$_3$CL-*g*-Gluco)-*b*-PCL was added to the Con A in the cuvette and the absorbance was recorded.

2.4. Cellular viability assay

The Promega CellTiter 96® AQueuous One Solution kit was used to determine cellular viability, following the manufacturer's instruction with minor modifications. In brief, HeLa cells were seeded in a 24-well plates (3×10^4 cells/well), cultured overnight, and then treated with the polymers at various concentrations (or with the DMSO vehicle) together with DMEM/F12 1:1 medium containing 1% FBS. After maintaining the cells for 24 h in a humidified 37 °C incubator supplied with 5% CO_2, the medium in each well was removed and replaced with 400 μL of warm PBS and 40 μL of the CellTiter 96® AQueuous One Solution. The cells were incubated at 37 °C for 1 h and then 110 μL of the supernatant from the wells was transferred to 96-well plates to measure absorbance at 485 nm using an ELISA reader (Hidex, Finland). Using these procedures, the cytotoxic effects of micelle-loaded and free doxorubicin (DOX) were also measured with 48 h incubation of the DOX samples with cells.

2.5. Uptake of DOX-loaded RO-(PαN$_3$CL-g-Gluco)-b-PCL micelles by HeLa cells

Cellular uptake of free drugs and drugs loaded in RO-(PαN$_3$CL-*g*-Gluco)-*b*-PCL micelles was visualized using a fluorescence microscope (IX71, Olympus, Japan). HeLa cells were seeded in 3.5 mm dishes (10^5 cells mL^{-1} density) and incubated overnight before adding 5 μg mL^{-1} free DOX or DOX loaded in RO-(PαN$_3$CL-*g*-Gluco)-*b*-PCL micelles; DMEM/F12 1:1 medium containing 1% FBS was added together with the DOX samples. The time course of cellular uptake of free and micelle-loaded DOX was examined using the red fluorescence channel and the results were quantified using Image J software (NIH, USA).

3. Results and discussion

3.1. Synthesis and characterization of RO-(PαN$_3$CL-g-Sugar)-b-PCL

The protocol for synthesizing RO-PαN$_3$CL-*b*-PCL, depicted in Scheme 1, was developed following previously published procedures, with modifications (Su, Yang, Leu, Hua, & Lee, 2012). For functionalizing aliphatic polyesters, chemical transformation by click reactions between alkynes and azides is facile because of the mild conditions and quantitative yields of the transformation (Geng et al., 2007). Here, CuI and Et_3N dissolved in DMF catalyzed the click reaction at 60 °C for 48 h, and 2 types of 4-pentynyl-sugars

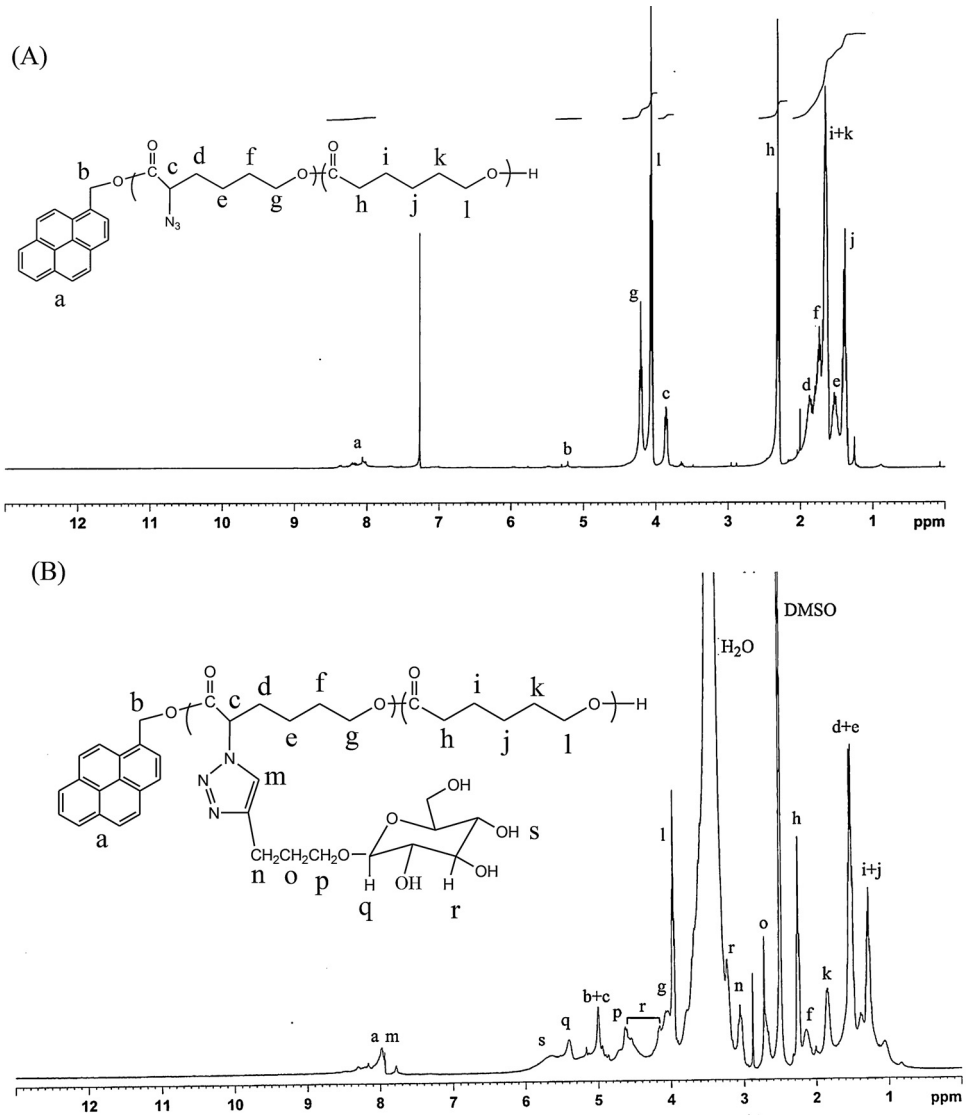

Fig. 1. Representative ^{1}H NMR spectroscopy (A) PMO-PαN$_3$CL$_{16}$-*b*-PCL$_{34}$, (B) PMO-(PαN$_3$CL$_{16}$-g-Gluco$_{13}$)-*b*-PCL$_{34}$.

(1-(4-pentynyl)-glucose, and 1-(4-pentynyl)-maltose) were chosen as model compounds for grafting onto PCL (Mereyala & Gurrala, 1998). Table 1 shows the cyclo-addition results. The $M_{n,GPC}$ was in agreement with $M_{n,NMR}$ and $M_{n,th}$. The grafting efficiency was between 48% and 82%.

In the FT-IR spectrum, the azide signal at 2104 cm^{-1} disappeared almost entirely, and the appearance of a new absorption peak at 1608 cm^{-1} reflected the vibration of the triazol unsaturated group, and confirmed the production a glycol-grafted polyester by the click reaction (Fig. S1C in supporting information). The

Table 1
Results of the grafting of RO-(PαN$_3$CL)-*b*-PCL with propargyl-sugar by click reaction.

Grafted copolymer[a]	[Sugar-O-(CH$_2$)$_3$C≡CH]/[RO-(PαN$_3$CL)-*b*-PCL]Molar ratio in the feed	[Sugar-O-(CH$_2$)$_3$C≡CH]/[RO-(PαN$_3$CL)-*b*-PCL]Molar ratio[b]	Grafting efficiency (%)	$M_{n,NMR}$[b]	$M_{n,th}$[c]	$M_{n,GPC}$[d]	M_w/M_n[d]
BzO-(PαN$_3$CL$_{24}$-*g*-Gluco$_{12}$)-*b*-PCL$_{23}$	24/1	12/1	50	9400	12,350	6360	1.18
BzO-(PαN$_3$CL$_{14}$-*g*- Gluco$_{10}$)-*b*-PCL$_{35}$	14/1	10/1	71	8730	9710	11,960	1.35
BzO-(PαN$_3$CL$_{14}$-g-Malto$_{10}$)-*b*-PCL$_{35}$	14/1	10/1	71	10,350	11,980	17,540	1.11
BzO-(PαN$_3$CL$_{27}$-*g*-Gluco$_{15}$)-*b*-PCL$_{29}$	27/1	15/1	56	11,290	15,110	17,220	1.24
BzO-(PαN$_3$CL$_{25}$-*g*-Gluco$_{12}$)-*b*-PCL$_{98}$	25/1	12/1	48	18,110	21,310	15,760	1.16
PMO-(PαN$_3$CL$_{16}$-*g*-Gluco$_{13}$)-*b*-PCL$_{34}$	16/1	13/1	79	9790	10,520	14,740	1.24
PMO-(PαN$_3$CL$_{37}$-*g*-Malto$_{30}$)-*b*-PCL$_{32}$	37/1	30/1	82	22,540	25,400	20,850	1.17
PMO-(PαN$_3$CL$_{16}$-*g*-Malto$_{10}$)-*b*-PCL$_{34}$	16/1	10/1	63	10,670	13,120	8350	1.19

[a] Abbreviations: Bz = benzyl; PM = 1-pyrenemethyl; Gluco = 4-pentynylglucose; Malto = 4-pentynylmalotose.
[b] Determine by ^{1}H NMR spectroscopy of RO-(PαN$_3$CL-*g*-Glyco)-*b*-PCL.
[c] $M_{n,th} = M_{n,\ RO\text{-}(P\alpha N3CL)\text{-}b\text{-}PCL} + M_{alkyne} \times$ [alkyne]/[RO-(PαN$_3$CL)-*b*-PCL]. (where $M_{n,RO\text{-}(P\alpha N3CL)\text{-}b\text{-}PCL}$ is the number-average molecular weight of RO-(PαN$_3$CL)-*b*-PCL, M_{alkyne} is the molecular weight of alkyne, [alkyne] is the alkyne molarity concentration, and [RO-(PαN$_3$CL)-*b*-PCL] is the polymer RO-(PαN$_3$CL)-*b*-PCL molarity concentration).
[d] Determined by GPC.

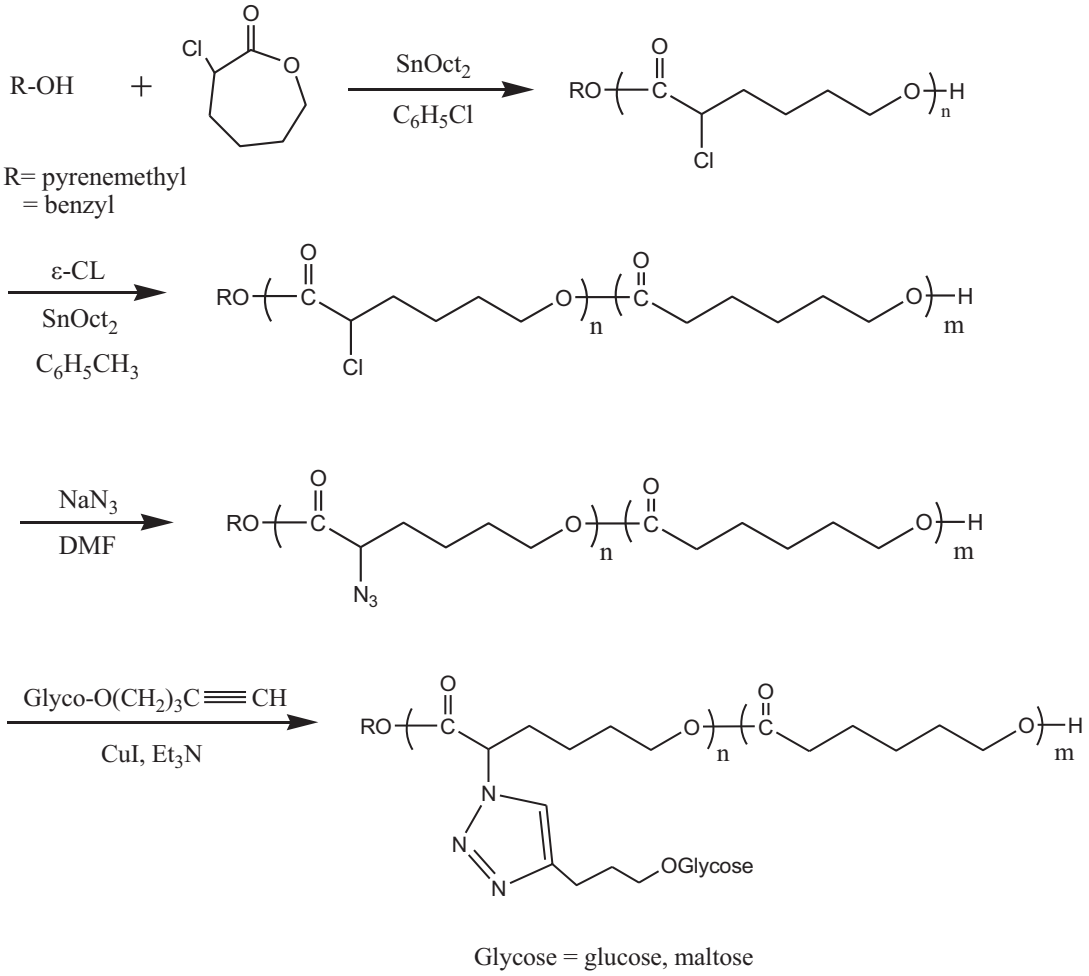

Scheme 1. Strategy for the synthesis of glyco-grafted RO-(PαN$_3$CL-*g*-Sugar)-*b*-PCL copolymer.

cyclo-addition was also confirmed by the disappearance of the CHN_3 proton resonance at 3.87 ppm in the ^{1}H NMR spectrum and the appearance of a new peak at 7.78 ppm (Fig. 1B), which represented a triazole proton. Additional new peaks were observed, and assigned to the protons of the grafted sugar. The [alkynyl-sugar]/[RO-PαN$_3$CL-*b*-PCL] molar ratio of the addition products, as calculated using $9I_m/I_a$ was lower than the molar ratio in the feed, which we attributed to a reduction in grafting caused by steric hindrance.

Fig. S2 (in supporting information) shows the UV–vis absorption and the fluorescence emission spectra of PMO-(PαN$_3$CL$_{16}$-*g*-Gluco$_{13}$)-*b*-PCL$_{34}$ in 0 1 wt% DMSO at room temperature. The UV–vis absorption spectrum of PMO-(PαN$_3$CL$_{16}$-*g*-Gluco$_{13}$)-*b*-PCL$_{34}$ showed typical absorption bands of pyrene at wavelength <400 nm; pyrene fluoresces in the 375–550 nm range in response to excitation at 317 nm. The fluorescence emission spectrum of PMO-(PαN$_3$CL$_{16}$-*g*-Gluco$_{13}$)-*b*-PCL$_{34}$ exhibited a broad excimer emission, which may be due to the influence of the local microenvironment on the spectral features of the pyrenyl groups.

3.2. Micelles of graft-block copolymers

The graft-block copolymers consist of hydrophilic PαN$_3$CL-g-Glucose, or PαN$_3$CL-g-Maltose blocks and hydrophobic PCLs, and the amphiphilic nature of the copolymers allows them to form micelles in water. The characteristics of the graft-block copolymer micelles in the aqueous phase, including their CMCs, were investigated using fluorescence techniques with pyrene serving as the probe.

In the excitation spectrum of pyrene (spectrum not shown), fluorescence intensity increased when the concentration of RO-(PαN$_3$CL-*g*-Sugar)-*b*-PCL was increased. The CMC values of the RO-(PαN$_3$CL-*g*-Sugar)-*b*-PCL graft-block copolymers were determined using a typical feature of the pyrene excitation spectrum, the red shift of the (0,0) band from 334 nm to 337 nm upon the uptake of pyrene into a micellar hydrophobic core. Fig. 2 shows the intensity ratios (I_{337}/I_{334}) of the pyrene excitation spectrum versus the logarithm of concentration of the RO-(PαN$_3$CL-*g*-Sugar)-*b*-PCL graft-block copolymers. CMCs were determined by drawing straight intersecting lines through the points at the lowest polymer concentrations, which lie on a nearly horizontal line, and the points on the rapidly rising part of the plot. Table 2 shows the CMCs of the graft-block copolymers with distinct block compositions; the CMCs ranged from 4.9 to 23.2 mg L^{-1}. When the hydrophobic segment is kept constant in a series of copolymers, increasing the hydrophilicity of the hydrophilic block lowers the CMC. The CMC values of glucose-grafted copolymers were lower than those of maltose-grafted copolymers, because glucose is more hydrophilic than maltose. Conversely, if the hydrophilicity of the hydrophilic block is kept constant, increasing the length of the hydrophobic segment lowers the CMC. The zeta potential of the grafted polymers ranged from −20.6 mV to −29.5 mV. The micelles generated with the sugar-grafted polymers were moderately stable, and

Table 2
Properties of IMC-loaded glycol-grafted RO-(PαN$_3$CL-*g*-glyco)-*b*-PCL copolymer micelles.

Copolymer	CMC (mg L^{-1})	Drug entrapment efficiency (%)[a]	Drug loading content (%)[a]	Micelle size (nm)		
				Blank/PDI	Zeta potential (mV)	With IMC/PDI Zeta potential (mV)
BzO-(PαN$_3$CL$_{14}$-*g*-Gluco$_{10}$)-*b*-PCL$_{35}$	4.9	20.5	41.0	23.2 ± 0.2/0.37	−20.6	63.1 ± 3.8/0.67 −9.3
BzO-(PαN$_3$CL$_{14}$-*g*-Malto$_{10}$)-*b*-PCL$_{35}$	5.5	13.0	26.0	21.0 ± 0.1/0.23	−27.1	
BzO-(PαN$_3$CL$_{27}$-*g*-Gluco$_{15}$)-*b*-PCL$_{29}$	23.2	14.7	29.4	24.7 ± 0.6/0.20	−27.1	113 ± 35.5/0.08 −32.7
BzO-(PαN$_3$CL$_{25}$-*g*-Gluco$_{12}$)-*b*-PCL$_{98}$	5.6	20.5	41.0	32.3 ± 0.2/0.14	−21.1	
PMO-(PαN$_3$CL$_{16}$-*g*-Gluco$_{13}$)-*b*-PCL$_{34}$	11.0	16.4	32.3	125.6 ± 44.2/0.12	−28.1	
PMO-(PαN$_3$CL$_{16}$-*g*-Malto$_{10}$)-*b*-PCL$_{34}$	15.2	8.1	16.2	91.3 ± 43.2/0.22	−29.5	

[a] Feed weight ratio IMC/polymer = 1/1.

the negative charge on the surface prevented the micelles from aggregating, which can be triggered by the absorption of serum proteins when administered in blood plasma.

Using DLS, the mean hydrodynamic diameters of the micelles without IMC were determined to range from 21 nm to 125 nm. When the concentration was fixed at 50 times the CMC value (50× CMC), the mean diameter of the micelles increased as the ratio of the lengths of the hydrophobic segment to that of the hydrophilic segment was increased. When the hydrophobic portion of the polymeric chain was increased, the particles generally became larger, whereas the incorporation of the drug increased micellar size only marginally. Fig. S3 (in supporting information) shows a similar trend in the morphology of micelles (not containing a stain). The empty and IMC-loaded micelles were nearly spherical and their diameters were slightly less than the hydrodynamic diameter obtained from the DLS experiment, which may be due to the micelles shrinking and collapsing after drying. The mean hydrodynamic diameter of IMC-loaded micelles ranged from 63 nm to 113 nm, which is less than the 200 nm diameter at which micellar uptake by reticuloendothelial cells becomes impaired.

3.3. Evaluation of drug-loading efficiency and drug content of micelles

IMC, a common non-steroidal anti-inflammatory drug, was selected to investigate how drug-loading efficiency is affected by the grafting sugars and the compositions of the copolymers. The percentages of drug-loading content (% DLC) and drug-entrapment efficiency (% DEE) were evaluated according to Eqs. (1) and (2). The amount of IMC incorporated into graft-block RO-(PαN$_3$CL-*g*-Sugar)-*b*-PCL micelles was calculated by measuring the absorbance after removing free IMC by filtration. The DEE and DLC of IMC-loaded micelles are shown in Table 2. At a constant feed-weight ratio (1/1), DEE and DLC increased with an increase in the hydrophilicity of the hydrophilic block and with the lengthening of the hydrophobic segments. Increasing micellar stability also enhanced the amount of drug entrapped in the micelles. Moreover, the DEE and DLC values of micelles with glucose-grafted polymers were higher than those of micelles with maltose-grafted polymers.

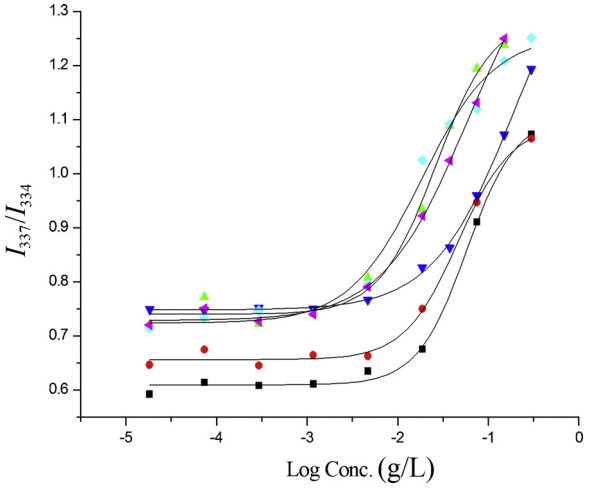

Fig. 2. Plot of I_{337}/I_{334} intensity ratio (from pyrene excitation spectra; concentration = 6.1×10^{-7} M) versus the logarithm of concentration (log C) for (■) PMO-(PαN$_3$CL$_{16}$-*g*-Malto$_{10}$)-*b*-PCL$_{34}$, (●) PMO-(PαN$_3$CL$_{16}$-*g*-Gluco$_{13}$)-*b*-PCL$_{34}$, (▼) BzO-(PαN$_3$CL$_{27}$-*g*-Gluco$_{15}$)-*b*-PCL$_{29}$, (◀) BzO-(PαN$_3$CL$_{14}$-*g*-Malto$_{10}$)-*b*-PCL$_{35}$, (◆) BzO-(PαN$_3$CL$_{14}$-*g*-Gluco$_{10}$)-*b*-PCL$_{35}$, (▲) BzO-(PαN$_3$CL$_{25}$-*g*-Gluco$_{12}$)-*b*-PCL$_{98}$. pyrene.

3.4. In vitro release of IMC

To investigate the effects of polymer composition on drug release, tests were conducted at 37 °C with various IMC-loaded RO-(PαN$_3$CL-*g*-Sugar)-*b*-PCL micelles. Fig. 3 shows that the IMC-loaded RO-(PαN$_3$CL-*g*-Sugar)-*b*-PCL micelles exhibited robust and sustained drug-release patterns, with the release of drugs becoming faster with an increase in the hydrophilicity of the hydrophilic blocks and a shortening of the hydrophobic segments. Increasing the hydrophilicity of the hydrophilic block enhanced the hydrophilicity of the micelles and accelerated the released of drugs. IMC was released faster by RO-(PαN$_3$CL-*g*-Gluco)-*b*-PCL than by RO-(PαN$_3$CL-*g*-Malto)-*b*-PCL, which can be attributed to glucose being more hydrophilic than maltose. These findings indicate that varying the length of the hydrophilic segment and the grafted sugars modulated the extent of drug released from the micelles. After an initial burst, the drug-release rate reached a plateau, suggesting that IMC-loaded micelles are stable under physiological conditions.

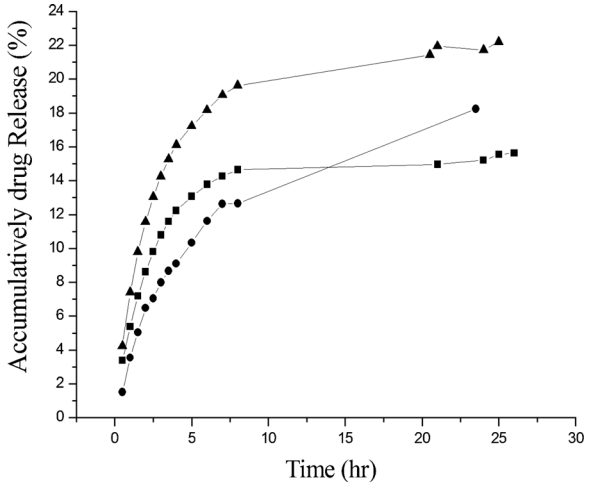

Fig. 3. IMC release from the micelles of BzO-(PαN$_3$CL$_{14}$-*g*-Gluco$_{10}$)-*b*-PCL$_{35}$ (▲), BzO-(PαN$_3$CL$_{25}$-*g*-Gluco$_{12}$)-*b*-PCL$_{98}$ (●), and BzO-(PαN$_3$CL$_{14}$-*g*-Malto$_{10}$)-*b*-PCL$_{35}$ (■) in PBS (pH 7.4) at 37 °C.

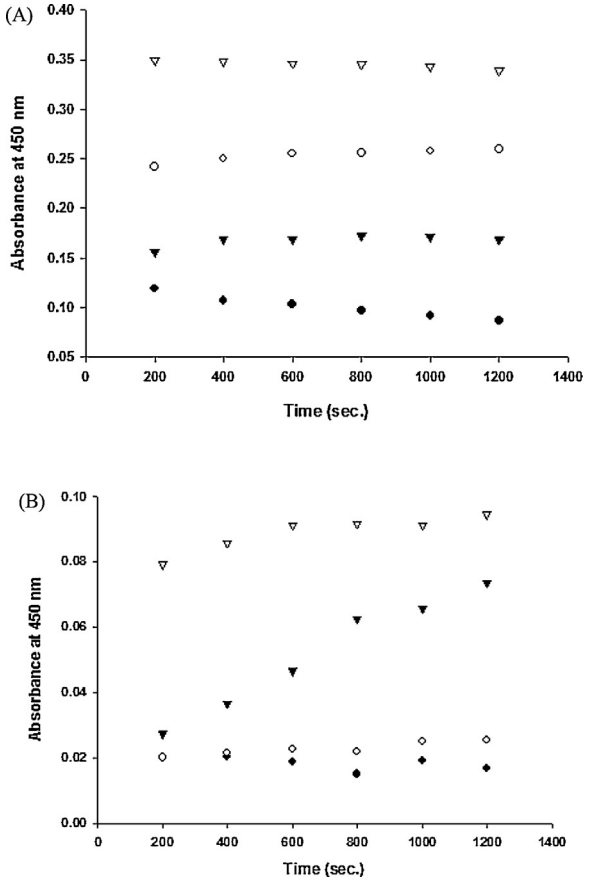

Fig. 4. The absorbance (450 nm) of the (A) BzO-(PαN$_3$CL$_{27}$-*g*-Gluco$_{15}$)-*b*-PCL$_{29}$, and (B) BzO-(PαN$_3$CL$_{14}$-*g*-Gluco$_{10}$)-*b*-PCL$_{35}$ solution upon reaction with lectin Con A (2 mg mL^{-1}) in PBS buffer: (▽) polymer concentration 0.2 mg mL^{-1} with lectin Con A, (○) polymer concentration 0.2 mg mL^{-1} without lectin Con A, (▼) polymer concentration 0.1 mg mL^{-1} with lectin Con A, (●) polymer concentration 0.1 mg mL^{-1} without lectin Con A.

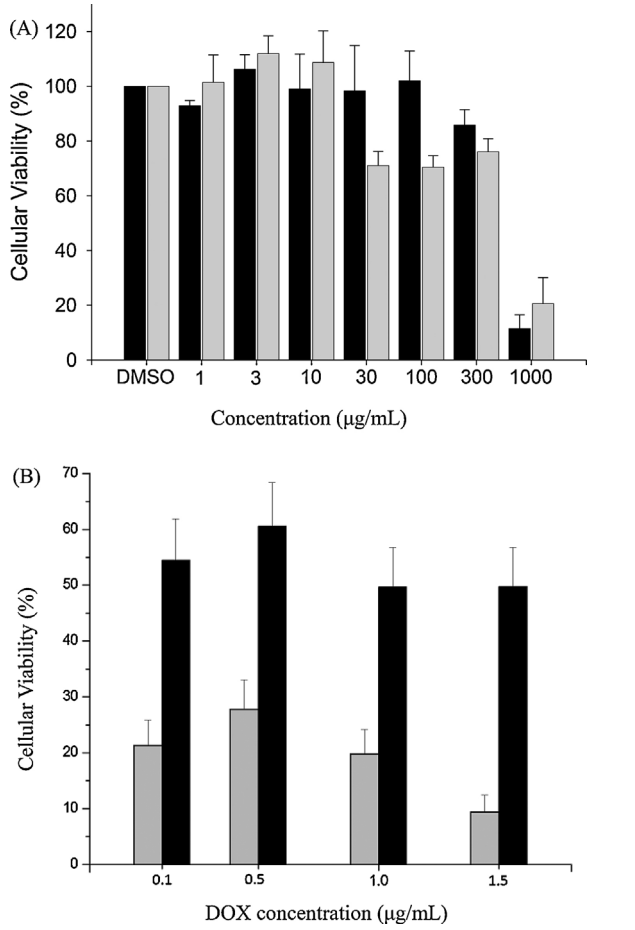

Fig. 5. Cellular viabilities of the HeLa cells after incubated for 48 h. (A) with BzO-(PαN$_3$CL$_{14}$-*g*-Gluco$_{10}$)-*b*-PCL$_{35}$ (black) and BzO-(PαN$_3$CL$_{27}$-*g*-Gluco$_{15}$)-*b*-PCL$_{29}$ (gray) of various concentrations, (B) with DOX-loaded BzO-(PαN$_3$CL$_{14}$-*g*-Gluco$_{10}$)-*b*-PCL$_{35}$ micelle (black) and free DOX (gray) of various concentrations. Data are shown as mean ± S.E. (n = 3).

3.5. Carbohydrate-lectin binding

The ability of the synthesized RO-(PαN$_3$CL-*g*-Sugar)-*b*-PCL to interact with biological systems was assessed. Carbohydrates-lectin binding plays key roles in biological recognition, and although the exact mechanism of this carbohydrate-lectin interaction is not completely understood, the interaction is highly specific and noncovalent. Thus, in vitro evaluation of carbohydrate-lectin binding is a first test of the ability of synthetic RO-(PαN$_3$CL-*g*-Sugar)-*b*-PCL to interact with biological systems, which may be relevant to the development of materials for drug delivery, tissue engineering, and other biomedical applications. Typically, tests of carbohydrate-lectin binding are conducted by mixing the RO-(PαN$_3$CL-*g*-Sugar)-*b*-PCL with a lectin that is selective for the sugar conjugated to the polymer (Ambrosi, Cameron, & Davis, 2005; Moine et al., 2010). A positive result is indicated by the appearance of a precipitate that is generated by the aggregation of lectins, which is measured as a reduction in the transparency of the solution. Because Con A is a lectin that selectively binds glucosyl residues, we examined the change in absorbance at 450 nm of solutions of RO-(PαN$_3$CL-*g*-Gluco)-*b*-PCL mixed with Con A. Fig. 4 shows that the absorbance (i.e., turbidity) was greater at higher concentrations of RO-(PαN$_3$CL-*g*-Gluco)-*b*-PCL because of the formation of larger aggregates. As a control experiment, PBS buffer without the glycopolymer was added to Con A: only a slight change in absorbance was detected (Huang et al., 2010), which was considerably less than the change in the sample containing glycopolymers. These experiments confirmed that RO-(PαN$_3$CL-*g*-Gluco)-*b*-PCL synthesized by the "click" coupling of glucose to RO-PαN$_3$CL-*b*-PCL enables bio-recognition by the glycopolymer micelles. The lectin binding was selective and, depending on the concentration, almost instantaneous. Notably, we observed no adverse effects of the triazole ring on the binding of the lectin.

3.6. Cytotoxicity of glucosylated copolymers and DOX-loaded micelles

To investigate the toxicity of the glucosylated RO-(PαN$_3$CL-*g*-Gluco)-*b*-PCL, we use the Promega MTS CellTiter 96® kit to measure cellular viabilities after treatment with BzO-(PαN$_3$CL$_{14}$-*g*-Gluco$_{10}$)-*b*-PCL$_{35}$ and BzO-(PαN$_3$CL$_{27}$-*g*-Gluco$_{15}$)-*b*-PCL$_{29}$ at various concentrations. HeLa cells were seeded in 24-well plates (3×10^4 cells/well) and incubated overnight, after which the culture medium was replaced with DMEM containing 1% FBS. Next, 1–1000 μg mL^{-1} of BzO-(PαN$_3$CL$_{14}$-*g*-Gluco$_{10}$)-*b*-PCL$_{35}$, BzO-(PαN$_3$CL$_{27}$-*g*-Gluco$_{15}$)-*b*-PCL$_{29}$, or the DMSO vehicle, was added; after incubation for 48 h, the medium in each well was removed, and the MTS reagent was added. The cells were incubated for 1–4 h to allow the bio-reduction of MTS into its formazan product, which can be measured by absorbance at 485 nm and which is directly proportional to the number of living cells in a culture. Neither BzO-(PαN$_3$CL$_{14}$-*g*-Gluco$_{10}$)-*b*-PCL$_{35}$ nor BzO-(PαN$_3$CL$_{27}$-*g*-Gluco$_{15}$)-*b*-PCL$_{29}$ inhibited cellular viability at concentrations

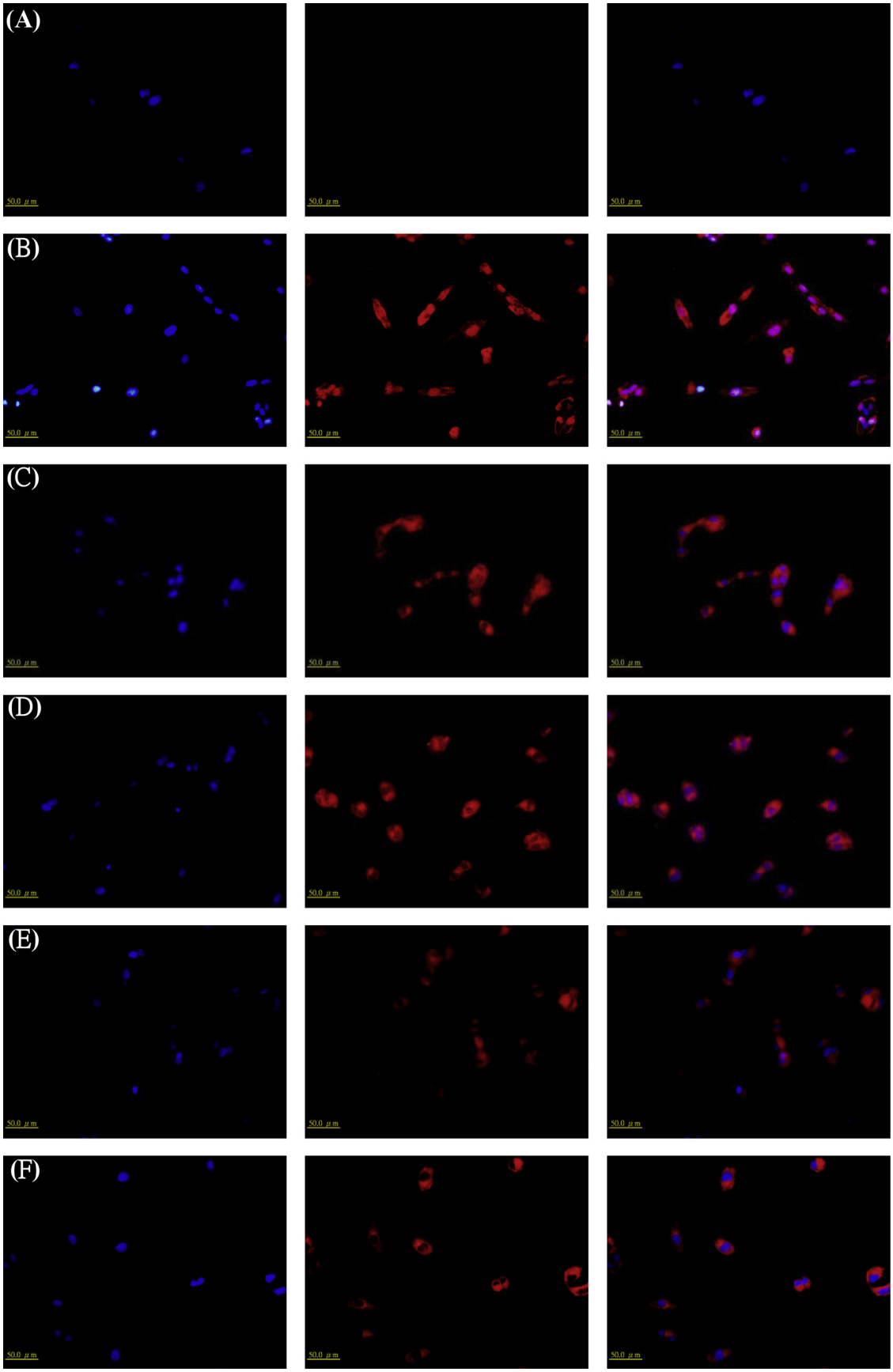

Fig. 6. Fluorescent microscopic images of HeLa cells incubated with free DOX (1.5 μg mL^{-1}) or DOX-loaded micelles for various time intervals: (A) free DOX, 5 min; (B) free DOX 1 h; (C) BzO-(PαN$_3$CL$_{14}$-*g*-Gluco$_{10}$)-*b*-PCL$_{35}$, 5 min; (D) BzO-(PαN$_3$CL$_{14}$-*g*-Gluco$_{10}$)-*b*-PCL$_{35}$, 1 h; (E) BzO-(PαN$_3$CL$_{27}$-*g*-Gluco$_{15}$)-*b*-PCL$_{29}$, 5 min; (F) BzO-(PαN$_3$CL$_{27}$-*g*-Gluco$_{15}$)-*b*-PCL$_{29}$, 1 h. For each row, images for left to right show the cells with hoechst 33342 nuclear staining, DOX fluorescence, and the merged image.

below 10 μg mL^{-1}. Between 30 and 300 μg mL^{-1} BzO-(PαN$_3$CL$_{14}$-*g*-Gluco$_{10}$)-*b*-PCL$_{35}$ still showed little cytotoxicity and 85% of the HeLa cells remained viable, whereas BzO-(PαN$_3$CL$_{27}$-*g*-Gluco$_{15}$)-*b*-PCL$_{29}$, killed approximately 30% of the cells; both glucosylated polymers were highly toxic cells at 1000 μg mL^{-1} (Fig. 5A). These data suggest that glucosylated RO-(PαN$_3$CL-*g*-Gluco)-*b*-PCL polymers are nontoxic at low to moderate concentrations.

The cytotoxicity against HeLa cells for the free DOX and DOX-loaded micelles was also determined by MTS assay. Fig. 5B show the viability of HeLa cells in the presence of free DOX and DOX-loaded BzO-(PαN$_3$CL$_{14}$-*g*-Gluco$_{10}$)-*b*-PCL$_{35}$ micelles. The cell viability was dose-dependent, and DOX-loaded BzO-(PαN$_3$CL$_{14}$-*g*-Gluco$_{10}$)-*b*-PCL$_{35}$ micelles exhibited much lower cytotoxicity compared to free DOX, which was most likely due to the slower release of DOX from micelles and the delayed nuclear uptake of DOX in HeLa cells.

3.7. Cellular internalization of DOX-loaded micelles

Polymeric micelles can potentially deliver various chemotherapeutic drugs to malignant tumors, including paclitaxel, cisplatin, SN-38, and DOX (Matsumura & Kataoka, 2009; Oerlemans et al., 2010). Because of its intrinsic fluorescence, DOX is commonly used as a probe for visualizing micellare uptake and the distribution of drugs (Dai et al., 2008; Jin et al., 2011; Shuai, Ai, Nasongkla, Kim, & Gao, 2004). To test the ability of micelles formed by our glucosylated copolymers to deliver drugs into cancer cells, DOX was incorporated into BzO-(PαN$_3$CL$_{14}$-*g*-Gluco$_{10}$)-*b*-PCL$_{35}$ and BzO-(PαN$_3$CL$_{27}$-*g*-Gluco$_{15}$)-*b*-PCL$_{29}$ polymer micelles using the dialysis method (Dai et al., 2008), with slight modifications in dialysis time and MWCO (see Section 2 for details). We selected HeLa cells because they are derived from a human cervical cancer. The lyophized, drug-loaded micelles were dissolved in DMEM containing 1% FBS and added to HeLa cells seeded in a 35 mm dish (1.0×10^5 cells/dish) for 5 min and 1 h. After the times indicated in Fig. 6B, cells were fixed using 4% paraformaldehyde and the nuclei were stained with Hoechst 33342, which emits blue fluorescence under UV excitation. Observation of the samples under a fluorescence microscope revealed that free DOX moved through the cytoplasm and deposited at nuclei in 1 h, which could be due to the inherent tendency of free DOX to translocate into nuclei (Sui, Liu, & Shen, 2011). The uptake of free DOX was marked by slow entry into cells, with little DOX fluorescence detected after 5 min exposure of cells to the drug (Fig. 6A). In contrast, DOX loaded in both BzO-(PαN$_3$CL$_{14}$-*g*-Gluco$_{10}$)-*b*-PCL$_{35}$ and BzO-(PαN$_3$CL$_{27}$-*g*-Gluco$_{15}$)-*b*-PCL$_{29}$ micelles accumulated rapidly in cells, with the DOX fluorescence being distributed mainly in the cytoplasm and appearing weakly in the nuclei (Fig. 6C–F).

Flow cytometry was used to further compare the time-dependent changes in intracellular fluorescence of free and micelle-loaded DOX. HeLa cells (3.0×10^5 cells/well) were seeded in a 6-well culture plates and incubated overnight. After treating the cells with free DOX or DOX-loaded BzO-(PαN$_3$CL$_{14}$-*g*-Gluco$_{10}$)-*b*-PCL$_{35}$ and BzO-(PαN$_3$CL$_{27}$-*g*-Gluco$_{15}$)-*b*-PCL$_{29}$ micelles for specific time intervals, cells were trypinized, fixed using paraformaldehyde, and examined by flow cytometry. The overlay histogram of intracellular fluorescence of DOX for the BzO-(PαN$_3$CL$_{14}$-*g*-Gluco$_{10}$)-*b*-PCL$_{35}$ and BzO-(PαN$_3$CL$_{27}$-*g*-Gluco$_{15}$)-*b*-PCL$_{29}$ DOX-loaded micelles (Fig. 7A), clearly demonstrates that both micelles entered cells rapidly, and that the intracellular concentration of DOX rose continuously for 1 h. Plotting the calculated mean fluorescence intensity values against DOX uptake (Fig. 7B) revealed that although the amount of intracellular DOX increased with time in all three cases, substantial amounts of DOX entered cells within 5 min only when encapsulated in micelles. These results and the

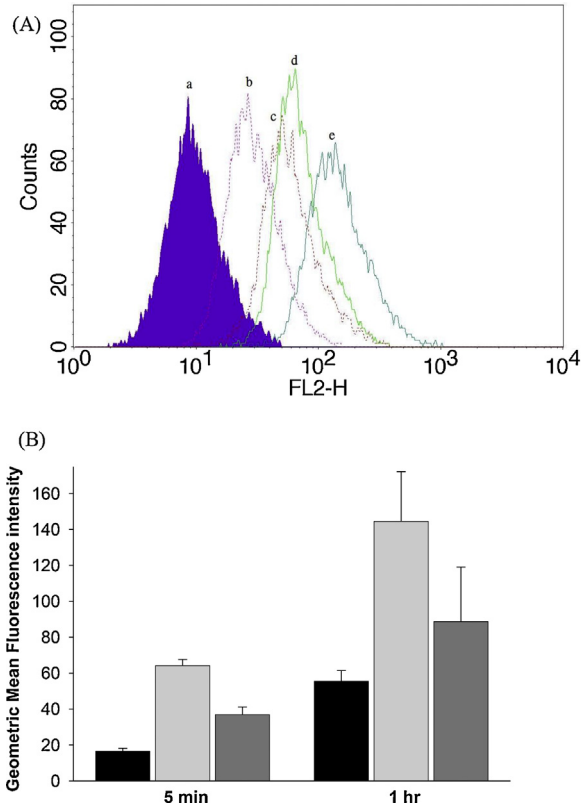

Fig. 7. (A) Flow cytometric histogram profiles of HeLa cells treated with DOX-loaded BzO-(PαN$_3$CL$_{14}$-*g*-Gluco$_{10}$)-*b*-PCL$_{35}$ and BzO-(PαN$_3$CL$_{27}$-*g*-Gluco$_{15}$)-*b*-PCL$_{29}$ micelles for different time intervals: a. Basal cellular fluorescence level; b. BzO-(PαN$_3$CL$_{27}$-*g*-Gluco$_{15}$)-*b*-PCL$_{29}$, 5 min; c. BzO-(PαN$_3$CL$_{27}$-*g*-Gluco$_{15}$)-*b*-PCL$_{29}$, 1 h; d. BzO-(PαN$_3$CL$_{14}$-*g*-Gluco$_{10}$)-*b*-PCL$_{35}$, 5 min; e. BzO-(PαN$_3$CL$_{14}$-*g*-Gluco$_{10}$)-*b*-PCL$_{35}$, 1 h. (B) Geometric mean fluorescence intensities of free DOX (black), DOX-loaded BzO-(PαN$_3$CL$_{14}$-*g*-Gluco$_{10}$)-*b*-PCL$_{35}$ (light gray), and DOX-loaded BzO-(PαN$_3$CL$_{27}$-*g*-Gluco$_{15}$)-*b*-PCL$_{29}$ (gray). Data are shown as mean ± S.E. ($n = 3$).

distribution profiles shown in Figs. 6C–F suggests that DOX-loaded micelles readily enter cells through endocytosis, as previously indicated (Jin et al., 2011; Shuai et al., 2004; Wang et al., 2011; Yan et al., 2011).

3.8. Investigation of the endocytic entry routes

Endocytosis is the de novo production of internal cellular membranes, together with integral membrane components, from the plasma membrane lipid bilayers (Doherty & McMahon, 2009; Kumari, Mg, & Mayor, 2010). Clathrin-mediated endocytosis (CME), caveolae-mediated endocytosis (CvME), and macropinocytosis are the major endocytic pathways responsible for the entry of "nanocarriers" into non-phagocytic cells (Hillaireau & Couvreur, 2009). The preferred entry route for a nanocarrier depends on the characteristics of the nanocarrier, such as size, surface charge, and surface coating (Gratton et al., 2008). To identify the endocytic pathways involved in the cellular uptake of drug-loaded glucosylated RO-(PαN$_3$CL-*g*-Gluco)-*b*-PCL micelles, we used specific biochemical inhibitors of endocytosis. HeLa cells seeded in 6-well plates were pretreated with inhibitors of endocytosis for 30 min, and then treated with DOX-loaded micelles of BzO-(PαN$_3$CL$_{14}$-*g*-Gluco$_{10}$)-*b*-PCL$_{35}$ or BzO-(PαN$_3$CL$_{27}$-*g*-Gluco$_{15}$)-*b*-PCL$_{29}$ in the presence of the same inhibitor used in the pretreatment. DOX fluorescence inside the cells was measured and analyzed using flow cytometry and calculated as the percentage of uptake relative to the control (cells treated with DOX-loaded micelles in the absence of inhibitors) (Fig. 8). CME is inhibited by chlorpromazine,

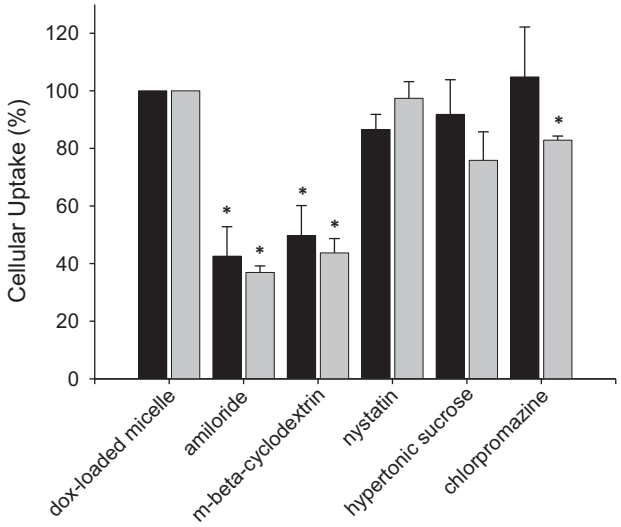

Fig. 8. The effects of endocytosis inhibitors on cellular uptake of DOX-loaded BzO-(PαN$_3$CL$_{14}$-*g*-Gluco$_{10}$)-*b*-PCL$_{35}$ (black) and BzO-(PαN$_3$CL$_{27}$-*g*-Gluco$_{15}$)-*b*-PCL$_{29}$ (gray) micelles. HeLa cells were pretreated for 30 min in DMEM + 1% FBS at 37 °C and 5% CO_2 alone, or with amiloride (4 mM), m-β-cyclodextrin (10 mM), nystatin (90 μM), sucrose (0.5 M), and chlorpromazine (10 μM). The previous media were then removed and replaced with DOX-loaded BzO-(PαN$_3$CL$_{14}$-*g*-Gluco$_{10}$)-*b*-PCL$_{35}$ or BzO-(PαN$_3$CL$_{27}$-*g*-Gluco$_{15}$)-*b*-PCL$_{29}$ medium which contained the identical inhibitors as mentioned above. After one-hour incubation, the cells were collected and analyzed with flow cytometry. Geometric mean fluorescence % of each group was subsequently calculated. Data are shown as mean ± S.E. ($n = 3$; the * $P \leq 0.05$, as determined with Student's *t*-test).

and hypertonic sucrose; chlorpromazine interferes with the functions of clathrin and the AP2 adaptor complex, whereas hypertonic sucrose disperses clathrin lattices on the plasma membrane (Ivanov, 2008). Neither chlorpromazine nor hypertonic sucrose blocked the uptake of DOX-loaded BzO-(PαN$_3$CL$_{14}$-*g*-Gluco$_{10}$)-*b*-PCL$_{35}$ micelles, but chlorpromazine weakly inhibited the uptake of DOX-loaded BzO-(PαN$_3$CL$_{27}$-*g*-Gluco$_{15}$)-*b*-PCL$_{29}$ micelles. Thus, CME may play a minor role in the uptake of glucosylated RO-(PαN$_3$CL-*g*-Gluco)-*b*-PCL. Nystatin and MβCD act on the cholesterol in the cell membrane to inhibit CvME, although MβCD may also impede macropinocytosis (Fernando et al., 2010). Whereas nystatin had no detectable effect on micellar uptake, MβCD inhibited the uptake of both BzO-(PαN$_3$CL$_{14}$-*g*-Gluco$_{10}$)-*b*-PCL$_{35}$ and BzO-(PαN$_3$CL$_{27}$-*g*-Gluco$_{15}$)-*b*-PCL$_{29}$ DOX-loaded micelles by approximately 50% (Fig. 8). These results suggested that MβCD hindered macropinocytosis, and not CvME, a notion that was confirmed by amiloride, which inhibits macropinocytosis by blocking the activity of the Na^+/H^+ exchanger. Treatment with amiloride repressed the cellular uptake of both types of micelles, to a similar extent as the administration of MβCD. These results support the conclusions that endocytosis plays a central role in the cellular uptake of glucosylated RO-(PαN$_3$CL-*g*-Gluco)-*b*-PCL DOX-loaded micelles, and that macropinocytosis, but not CME or CvME, mediates micellar entry into HeLa cells.

4. Conclusions

Amphiphilic block-graft poly(ε-caprolactone)s bearing pendent sugar moieties were synthesized by Huisgen [3+2] cyclo-addition of alkynyl-functional sugar derivative to the azido groups of RO-PαN$_3$CL-*b*-PCL. The formation of micelles by these amphiphilic polymers was confirmed using fluorescence probes and DLS. Increase in the length of the hydrophobic segment or in the hydrophilicity of the hydrophilic segment of the polymers lowered CMC values. Rapid and selective bio-recognition by micelles was demonstrated using lectin-clustering experiments. Importantly, DOX-loaded in micelles was more efficiently internalized by HeLa cells than free DOX, and micelle-loaded DOX, taken up by endocytosis, reached intracellular compartments and entered the nucleus.

Acknowledgements

This research was supported by Grants from Chang Gung University (UMRPD5B0081) and Chang Gung Memorial Hospital (CMRPD5B0012).

Appendix A. Supplementary data

Supplementary data associated with this article can be found, in the online version, at http://dx.doi.org/10.1016/j.carbpol.2013.08.098.

References

Ambrosi, M., Cameron, N. R., & Davis, B. G. (2005). Lectins: tools for the molecular understanding of the glycocode. *Organic & Biomolecular Chemistry*, *3*, 1593–1608.
Bertozzi, C. R., & Kiessling, L. (2001). Chemical glycobiology. *Science*, *291*(5512), 2357–2364.
Bordege, V., Munoz-Bonilla, A., Cuervo-Rodriguez, R., Sanchez-Chaves, M., & Fernandez-Garcia, M. (2011). Gluconolactone-derivated polymers: Copolymerization, thermal properties, and their potential use as polymeric surfactants. *Journal of Polymer Science Part A: Polymer Chemistry*, *49*, 526–536.
Cerrada, M. L., Bordegé, V., Muñoz-Bonilla, A., León, O., Cuervo-Rodríguez, R., Sánchez-Chaves, M., & Fernández-García, M. (2013). Amphiphilic polymers bearing gluconolactone moieties: Synthesis and long side-chain crystalline behavior. *Carbohydrate Polymers*, *94*, 755–764.
Dai, X., Yue, Z., Eccleston, M. E., Swartling, J., Slater, N. K., & Kaminski, C. F. (2008). Fluorescence intensity and lifetime imaging of free and micellar-encapsulated doxorubicin in living cells. *Nanomedicine*, *4*, 49–56.
Doherty, G. J., & McMahon, H. T. (2009). Mechanisms of endocytosis. *Annual Review of Biochemistry*, *78*, 857–902.
Fernando, L. P., Kandel, P. K., Yu, J., McNeill, J., Ackroyd, P. C., & Christensen, K. A. (2010). Mechanism of cellular uptake of highly fluorescent conjugated polymer nanoparticles. *Biomacromolecules*, *11*, 2675–2682.
Geng, J., Mantovani, G., Tao, L., Nicolas, J., Chen, G., Wallis, R., Mitchell, D. A., Johnson Benjamin, R. G., Evans, S. D., & Haddleton, D. M. (2007). Site-directed conjugation of clicked glycopolymers to form glycoprotein mimics: Binding to mammalian lectin and induction of immunological function. *Journal of the American Chemical Society*, *129*, 15156–15163.
Gratton, S. E., Ropp, P. A., Pohlhaus, P. D., Luft, J. C., Madden, V. J., Napier, M. E., & DeSimone, J. M. (2008). The effect of particle design on cellular internalization pathways. *Proceedings of the National Academy of Sciences of the United States of America*, *105*, 11613–11618.
Hillaireau, H., & Couvreur, P. (2009). Nanocarriers' entry into the cell: relevance to drug delivery. *Cellular and Molecular Life Sciences*, *66*, 2873–2896.
Huang, J., Habraken, G., Audouin, F., & Heise, A. (2010). Hydrolytically stable bioactive synthetic glycopeptides homo- and copolymers by combination of NCA polymerization and click reaction. *Macromolecules*, *43*, 6050–6057.
Ivanov, A. I. (2008). Pharmacological inhibition of endocytic pathways: Is it specific enough to be useful? *Methods in Molecular Biology*, *440*, 15–33.
Jin, Y., Song, L., Su, Y., Zhu, L., Pang, Y., Qiu, F., Tong, G., Yan, D., Zhu, B., & Zhu, X. (2011). Oxime linkage: A robust tool for the design of pH-sensitive polymeric drug carriers. *Biomacromolecules*, *12*, 3460–3468.
Jubeli, E., Moine, L., & Barratt, G. (2010). Synthesis, characterization, and molecular recognition of sugar-functionalized nanoparticles prepared by a combination of ROP, ATRP and click chemistry. *Journal of Polymer Science Part A: Polymer Chemistry*, *48*, 3178–3187.
Jutz, G., & Böker, A. (2011). Bionanoparticles as functional macromolecular building blocks - A new class of nanomaterials. *Polymer*, *52*, 211–232.
Kim, J. C., Rho, Y., Kim, G., Kim, M., Kim, H., Kim, I. J., Kim, J. R., & Ree, M. (2013). New self-assembled brush glycopolymers: Synthesis, structure and properties. *Polymer Chemistry*, *4*, 2260–2271.
Krannig, K. S., & Schlaad, H. (2012). pH-responsive bioactive glycopolypeptides with enhanced helicity and solubility in aqueous solution. *Journal of the American Chemical Society*, *134*, 18542–18545.
Kumari, S., Mg, S., & Mayor, S. (2010). Endocytosis unplugged: multiple ways to enter the cell. *Cell Research*, *20*, 256–275.
Lee, R. S., & Peng, K. Y. (2012). Synthesis of glycopoly(pseudo amino acid)s and their interaction with lectins. *Reactive and Functional Polymers*, *72*, 564–573.
Lu, C., Shi, Q., Chen, X., Lu, T., Xie, Z., Hu, X., Ma, J., & Jing, X. (2007). Sugars-grafted aliphatic biodegradable poly(L-lactide-co-carbonate)s by click reaction and their specific interaction with lectin molecules. *Journal of Polymer Science Part A: Polymer Chemistry*, *45*, 3204–3217.

Matsumura, Y., & Kataoka, K. (2009). Preclinical and clinical studies of anticancer agent-incorporating polymer micelles. *Cancer Science*, *100*, 572–579.
Menon, S., & Das, S. (2012). A photoresponsive fluorescent glycopolymer. *Polymer Chemistry*, *3*, 2619–2624.
Mereyala, H. B., & Gurrala, S. R. (1998). A highly diastereoselective, practical synthesis of allyl, propargyl 2,3,4,6-tetra-O-acetyl-β-d-gluco, β-d-galactopyranosides and allyl, propargyl heptaacetyl-β-d-lactosides. *Carbohydrate Research*, *307*, 351–354.
Mikhail, A. S., & Allen, C. (2009). Block copolymer micelles for delivery of cancer therapy: Transport at the whole body, tissue and cellular levels. *Journal of Controlled Release*, *138*, 214–223.
Moughton, A. O., Hillmyer, M. A., & Lodge, T. P. (2011). Multicompartment block polymer micelles. *Macromolecules*, *45*, 2–19.
Oerlemans, C., Bult, W., Bos, M., Storm, G., Nijsen, J. F., & Hennink, W. E. (2010). Polymeric micelles in anticancer therapy: targeting, imaging and triggered release. *Pharmaceutical Research*, *27*, 2569–2589.
Polikarpov, N., Kaufmann, A., Kluge, J., Appelhans, D., & Voit, B. (2010). Investigation of dye glycopolymer and glycopolymer hydrogel interactions for development of multi-release system. *Journal of Controlled Release*, *148*, e66–e67.
Rajendran, L., Knölker, H. J., & Simons, K. (2010). Subcellular targeting strategies for drug design and celivery. *Nature Reviews*, *9*, 29–42.
Shuai, X., Ai, H., Nasongkla, N., Kim, S., & Gao, J. (2004). Micellar carriers based on block copolymers of poly(epsilon-caprolactone) and poly(ethylene glycol) for doxorubicin delivery. *Journal of Controlled Release*, *98*, 415–426.
Su, R. J., Yang, H. W., Leu, Y. L., Hua, M. Y., & Lee, R. S. (2012). Synthesis and characterization of amphiphilic functional polyesters by ring-opening polymerization and click reaction. *Reactive and Functional Polymers*, *72*, 36–44.
Sui, M., Liu, W., & Shen, Y. (2011). Nuclear drug delivery for cancer chemotherapy. *Journal of Controlled Release*, *155*, 227–236.
Sunasee, R., & Narain, R. (2013). Glycopolymers and glycol-nanoparticles in biomolecular recognition processes and vaccine development. *Macromolecular Bioscience*, *13*, 9–27.
Ting, S. R. S., Chen, G., & Stenzel, M. H. (2010). Synthesis of glycopolymers and their multivalent recognitions with lectins. *Polymer Chemistry*, *1*, 1392–1412.
Top, A., & Kiick, K. L. (2010). Multivalent protein polymers with controlled chemical and physical properties. *Advanced Drug Delivery Reviews*, *62*, 1530–1540.
Torchilin, V. P. (2007). Micellar nanocarriers: Pharmaceutical perspective. *Pharmaceutical Research*, *27*, 1–16.
Tunca, U. (2013). Triple click reaction strategy for macromolecular diversity. *Macromolecular Rapid Communications*, *34*, 38–46.
Tyrrell, Z. L., Shen, Y. Q., & Radosz, M. (2010). Fabrication of micellar nanoparticles for drug delivery through the self-assembly of block copolymers. *Progress in Polymer Science*, *35*, 1128–1143.
Wang, D., Su, Y., Jin, C., Zhu, B., Pang, Y., Zhu, L., Liu, J., Tu, C., Yan, D., & Zhu, X. (2011). Supramolecular copolymer micelles based on the complementary multiple hydrogen bonds of nucleobases for drug delivery. *Biomacromolecules*, *12*, 1370–1379.
Xiao, C., Zhao, C., He, P., Tang, Z., Chen, X., & Jing, X. (2010). Facile synthesis of glycopolypeptides by combination of ring-opening polymerization of an alkyne-substituted N-carbpxyanhydride and click glycosylation. *Macromolecular Rapid Communications*, *31*, 991–997.
Yan, J., Ye, Z., Chen, M., Liu, Z., Xiao, Y., Zhang, Y., Zhou, Y., Tan, W., & Lang, M. (2011). Fine tuning micellar core-forming block of poly(ethylene glycol)-block-poly(epsilon-caprolactone) amphiphilic copolymers based on chemical modification for the solubilization and delivery of doxorubicin. *Biomacromolecules*, *12*, 2562–2572.